Switching of Dirac-Fermion Mass at the Interface of Ultrathin Ferromagnet and Rashba Metal

K. Honma,[1] T. Sato,[1] S. Souma,[2] K. Sugawara,[2] Y. Tanaka,[1] and T. Takahashi[1,2]
[1]Department of Physics, Tohoku University, Sendai 980-8578, Japan
[2]WPI Research Center, Advanced Institute for Materials Research, Tohoku University, Sendai 980-8577, Japan
(Received 8 May 2015; revised manuscript received 11 November 2015; published 23 December 2015)

We have performed spin- and angle-resolved photoemission spectroscopy on tungsten (110) interfaced with an ultrathin iron (Fe) layer to study an influence of ferromagnetism on the Dirac-cone-like surface-interface states. We found an unexpectedly large energy gap of 340 meV at the Dirac point, and have succeeded in switching the Dirac-fermion mass by controlling the direction of Fe spins (in plane or out of plane) through tuning the thickness of the Fe overlayer or adsorbing oxygen on it. Such a manipulation of Dirac-fermion mass via the magnetic proximity effect opens a promising platform for realizing new spintronic devices utilizing a combination of exchange and Rashba-spin-orbit interactions.

DOI: 10.1103/PhysRevLett.115.266401 PACS numbers: 71.18.+y, 71.70.-d, 73.20.-r, 79.60.-i

Two-dimensional electron systems at the surface of three-dimensional topological insulators (TIs) and graphene have attracted particular attention not only in fundamental scientific interest but also in their potential applicability to new electronic devices [1–4]. These 2D systems are commonly characterized by massless Dirac fermions originating from relativistic motion of electrons, as described by the Dirac equation. Distinct from free electrons displaying simple parabolic energy dispersion, the 2D Dirac systems share peculiar electronic states called a Dirac cone, where linearly dispersive bands cross each other at a momentum called the Dirac point. While the characteristics of the Dirac cone between the 3D TIs and graphene are markedly different in the role of spin-orbit coupling (SOC) and the spin-degenerate or spin-split nature of energy bands, intriguingly, one of the central issues in both systems lies in the creation of an energy gap at the Dirac point (Dirac gap) which corresponds to introducing a mass term in the Dirac equation. This massive Dirac-fermion phase can be achieved by breaking time-reversal symmetry (TRS) (TI case) or sublattice symmetry (graphene case) and plays a key role for realizing novel quantum phenomena as highlighted by theoretical predictions of topological magnetoelectric effect and quantum anomalous Hall effect in the 3D TIs [5,6] and also by the intensive band gap engineering of graphene toward applications to semiconductor devices [7–9], whereas the realization of a sufficiently large Dirac-fermion mass is an experimental challenge. It is thus of particular importance to seek Dirac-cone states among various systems to discover new functionalities of materials.

The tungsten (110) surface hosts almost linearly dispersive Dirac-cone-like surface states at the Brillouin zone center [10], as revealed by recent spin- and angle-resolved photoemission spectroscopy (ARPES). This Dirac cone has a spin-split nature due to Rashba SOC at the surface, and is situated within a partial bulk-band gap caused by the SOC, similar to the SOC-induced band gap of the 3D TIs. The Dirac cone in W(110) mainly consists of d orbitals [10–14] unlike those of 3D TIs and graphene arising mainly from p electrons, giving rise to a large anisotropy in the Dirac-cone shape [11–14]. Since W(110) has a good interface matching with Fe [15–17], it provides an excellent platform for manipulating Dirac fermions by breaking TRS with ferromagnetism.

In this Letter, we report a spin-resolved ARPES study of Fe/W(110). We found a spin-split Dirac-cone-like interface states, whose Dirac-fermion mass can be switched by controlling the direction of Fe spins. The observed energy gap of 340 meV is the largest among any known SOC systems, demonstrating that the magnetic proximity effect is highly useful for the realization of exotic quantum phenomena and spintronic devices at room temperature.

A tungsten single crystal was cleaned by cycles of annealing in oxygen atmosphere of 10^{-7}–10^{-9} Torr at 1500 K and subsequent heating at 2300 K. After cleaning, we observed a sharp $c(1\times1)$ low-energy electron-diffraction (LEED) pattern. Fe films were deposited on the clean W(110) substrate in ultrahigh vacuum of 2×10^{-10} Torr at room temperature. The film thickness was controlled by the deposition time, and the calibration of the Fe coverage was carried out using a quartz-oscillator thickness monitor. We also evaluated the Fe coverage by observing satellite LEED spots which reflect coverage-dependent lattice relaxation [17] (see Supplemental Material [18]). All the films were annealed at 500 K after the Fe deposition. ARPES measurements were performed with the MBS-A1 electron analyzer, which is directly connected to the sample-preparation chamber. We used the He-Iα resonance line ($h\nu = 21.218$ eV) to excite photoelectrons. The energy resolution for the regular and spin-resolved ARPES measurements was set at 20 and

80 meV, respectively. The sample temperature was kept at 120 K during the measurements. We used the Sherman function value of 0.07 to obtain spin-resolved ARPES data.

Let us start by presenting the electronic states of Fe/W(110) with an accurate control of Fe-layer coverage d. As visible from the ARPES intensity plot of the energy distribution curves (EDCs) for pristine W(110) along the $\bar{\Gamma}-\bar{S}$ cut in Fig. 1(a), a nearly linearly dispersive x-shaped Dirac-cone band (Dirac point is located at 1.25 eV) is clearly resolved at the $\bar{\Gamma}$ point. Upon Fe deposition of 0.9 ML (monolayer), the Dirac-cone band appears to shift upward by 0.45 eV. These features are better illustrated in the second-derivative intensity plots in Fig. 1(b). A spin-resolved ARPES experiment with this sample [Fig. 1(c)] demonstrates an in-plane spin polarization antisymmetric with respect to the $\bar{\Gamma}$ point and negligible out-of-plane spin component, similarly to the surface states of pristine W(110) (note that we mainly observe spin signal from tungsten, since the sample is not magnetized and the Fe layer forms multiple magnetic domains leading to the zero net spin polarization of the Fe layer). This indicates that the Dirac cone exists even after interfacing ultrathin Fe layer (see Supplemental Material [18]), despite a marked change in the electrostatic potential. Survival of the Dirac cone is well depicted in the extracted band dispersions [Fig. 1(d)] where the interface Dirac-cone band keeps essentially the gapless x-shaped dispersion as in the pristine counterpart.

Important physics manifests itself when the Fe coverage becomes thicker than 1 ML. For $d = 1.7$ ML [Fig. 1(b)], we immediately notice that the Dirac-cone band splits into upper and lower branches separated by an unexpectedly large energy gap (Dirac gap) of 0.34 eV [Fig. 1(d); see also the second derivative plots in Fig. S2 of Supplemental Material [18]]. This indicates that the originally massless Dirac fermions acquire a mass upon a slight increase in d. Surprisingly, on further increasing d up to 2.7 ML, the energy gap again vanishes and the x-shaped band recovers [Figs. 1(b) and 1(d)]. Such a thickness-selective switching of massless-massive Dirac fermions is also visualized in the EDCs at the $\bar{\Gamma}$ point in Fig. 1(e) where the Dirac gap, as evidenced by the two-peaked feature, is only seen for $d = 1.3$–2.2 ML. Interestingly, the Dirac gap always keeps the same value irrespective of the coverage, suggesting that the gap originates from the 2-ML-thick Fe layer, consistent with the well-established growth mode of Fe overlayers on W(110) [15–17].

Having established the existence of the Dirac gap, a natural question arises as to the physical mechanism behind the mass acquisition of Dirac fermions. One plausible explanation is the hybridization between the Dirac-cone band and the quantized Fe 3d bands. Specifically, if the gap accidentally opens only for the 2-ML Fe film due to this band hybridization, it follows that the energy gap arises from an *accidental* overlap of the Dirac cone and Fe 3d

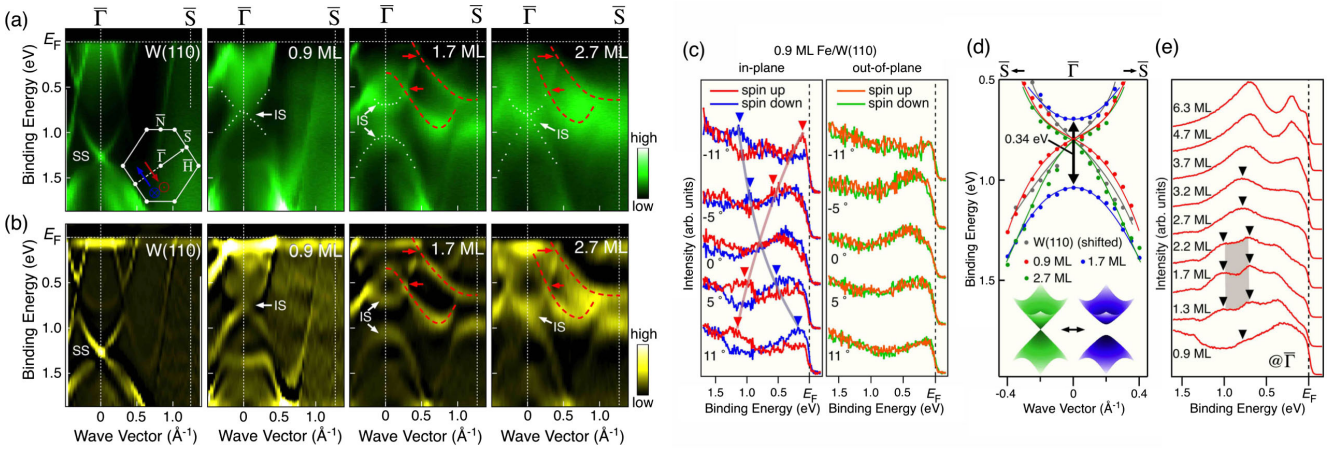

FIG. 1 (color online). (a),(b) ARPES intensity plots and corresponding second-derivative intensity of the energy distribution curves (EDCs), respectively, for Fe/W(110) with various Fe coverage ($d = 0$, 0.9, 1.7, and 2.7 ML), measured along the $\bar{\Gamma}$-$\bar{S}$ high-symmetry line in the bcc(110) surface Brillouin zone (inset) with the He-Iα line ($h\nu = 21.218$ eV) at $T = 120$ K. SS and IS indicate the surface and interface states, respectively. White dots represent the experimental energy dispersion of the gapless or gapped Dirac-cone-like bands [same as dots in (d)] extracted by tracing the peak position of the second derivative of the EDCs. Red curves for 1.7- and 2.7-ML films highlight the energy dispersion of the quantized Fe 3d bands, whereas the red arrows highlight the crossing points of the upper Dirac cone and the Fe 3d bands. (c) Spin-resolved EDCs around the $\bar{\Gamma}$ point of 0.9-ML Fe/W(110) for the in-plane (left) and out-of-plane (right) components. The peak position of the spin-resolved EDCs for the in-plane component is highlighted by triangles, while the band dispersion is guided by solid curves. Definition of the up- or down-spin direction is indicated in the surface Brillouine zone in (a). (d) Comparison of the experimental band dispersion of the Dirac-cone band (dots) for different Fe coverage. Solid curves are a guide to the eyes to trace the band dispersion. The band dispersion for pristine W(110) is shifted upward by 0.45 eV for better comparison. Switching of the Dirac gap in the 3D band dispersion is schematically illustrated. (e) Fe-coverage dependence of the EDC at the $\bar{\Gamma}$ point. Energy position of the Dirac-cone band is indicated by black triangles. Shaded area highlights the gapped energy region. Note that the Dirac-cone band is gradually smeared out upon increasing d and becomes indistinguishable from the Fe 3d peak for $d \geq 3.7$ ML.

bands. However, we do not observe any signature of the Fe 3d bands around the Dirac point [see Figs. 1(a) and 1(b)], which must be observed as a consequence of hybridization. Also, as visible in Figs. 1(a) and 1(b), the Fe 3d bands and the upper Dirac cone do not avoid crossing with each other away from $\bar{\Gamma}$ (see red arrows for 1.7- and 2.7-ML films). Moreover, despite the drastic difference in the gap-opening behavior of the Dirac cone, the energy dispersion of the Fe 3d bands is similar to each other between 1.7- and 2.7-ML films. All these observations are incompatible with the band-hybridization scenario. We also considered another possibility that the observed "upper Dirac-cone-like" feature in Figs. 1(a) and 1(b) is not the real upper Dirac cone, but is another W-derived interface state. However, this possibility is also unlikely, because both the band velocity and the spin texture in the Dirac-cone states are very similar between pristine W(110) and 0.9-ML film [Figs. 1(c) and 1(d)]. Therefore, the most natural explanation for the mass acquisition is the TRS breaking due to ferromagnetic order [19–21]. We therefore magnetized the Fe overlayer to form a single magnetic domain, and experimentally extracted the spin polarization of Fe. By closely inspecting the quantized electronlike Fe 3d band at the $\bar{\Gamma}$ point [Fig. 2(a)], we revealed that the spin vector for $d = 0.9$ ML is oriented in plane, as can be judged from the spin-resolved EDCs in Fig. 2(b), where the large in-plane spin polarization is detected near E_F in contrast to the negligible out-of-plane component [see also Fig. 2(c)] (note that the observed spin polarization is intrinsic to the Fe layer, since we detected a sign switch of the spin polarization upon reversing the magnetization direction). While a similar in-plane spin orientation was also observed for $d = 3.2$ ML, we found the absence of both in-plane and out-of-plane spin polarization for $d = 1.7$ ML [Fig. 2(d)]. This is well understood by the reported spin texture of the 2-ML Fe island [22–25]. According to the previous experimental studies with the spin-polarized scanning tunneling spectroscopy and the torsion oscillation magnetometry [22–25], 2-ML Fe on W(110) has a perpendicular magnetic anisotropy and each domain of the Fe islands has the out-of-plane magnetization, but adjacent domains couple antiferromagnetically to lead to zero net spin polarization [Fig. 2(c)]. This is in sharp contrast to the 1- and more-than-3-ML Fe films where the magnetic easy axis is aligned in plane $[1\bar{1}0]$ direction [16,26,27]. Therefore, it is strongly suggested from our ARPES experiment, corroborated by the previous studies, that the out-of-plane magnetic order is responsible for the mass acquisition of Dirac fermions for 2-ML Fe, whereas the Dirac fermions keep the massless nature when the in-plane magnetic order is stabilized for 1- and 3-ML Fe. This observation is consistent with the theoretical model incorporating an exchange interaction into the Dirac Hamiltonian [28]. It is also noted here that for 1- and 3-ML Fe we did not clearly observe an expected shift in the Dirac-cone position in momentum space with the in-plane

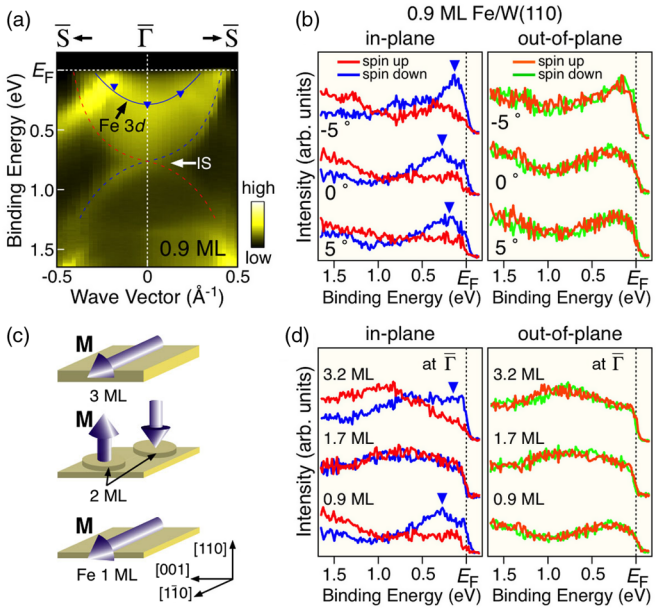

FIG. 2 (color online). (a) ARPES intensity plot around the $\bar{\Gamma}$ point of Fe/W(110) for $d = 0.9$ ML. Dashed and solid curves indicate the band dispersion of the Dirac cone and the quantized Fe 3d band, respectively. Blue triangles indicate the peak position of the spin-resolved EDCs in (b). (b) Spin-resolved EDCs for the in-plane (left) and out-of-plane (right) components of 0.9-ML Fe/W(110) measured at three representative k points around the $\bar{\Gamma}$-$\bar{S}$ point. Sample was magnetized along the $[1\bar{1}0]$ direction. Peak position of the down-spin EDCs for the in-plane component is indicated by triangles. (c) Schematic illustration of the thickness dependence of spin direction for Fe overlayers. Spin vector aligns in plane (the $[1\bar{1}0]$ direction) for the Fe thickness of 1 and 3 ML, whereas that of the 2-ML islands directs out of plane due to the perpendicular magnetic anisotropy [22–25]. (d) Thickness dependence of the spin-resolved EDCs at the $\bar{\Gamma}$ point for the in-plane (left) and out-of-plane (right) components.

magnetic order, which implies the possible anisotropy in the effective exchange-coupling strength at the Fe/W interface.

Besides the switching of Dirac-fermion mass by tuning the number of Fe layers, oxygen adsorption onto the Fe surface was found to create a similar effect. As displayed by a side-by-side comparison of ARPES intensity in Figs. 3(a) and 3(b), the originally gapped Dirac-cone band for $d \sim 1.5$ ML [Fig. 3(a)] transforms into an x-shaped gapless state [Fig. 3(b)] after the adsorption of 0.25-ML oxygen. This transition is well illustrated in the band dispersion [Fig. 3(c)] and the EDC at the $\bar{\Gamma}$ point [Fig. 3(d)], which resemble the mass switching behavior in the oxygen-free samples (Fig. 1). Our spin-resolved ARPES data [Fig. 3(e)] also suggest that the out-of-plane-oriented Fe spin for $d \sim 1.5$ ML rotates to the in-plane direction upon the oxygen adsorption, as inferred from a finite (negligible) difference between the in-plane up- and down-spin EDC for the oxygen-adsorbed (native) surface (note that similar spin reorientation due to residual-gas adsorption was

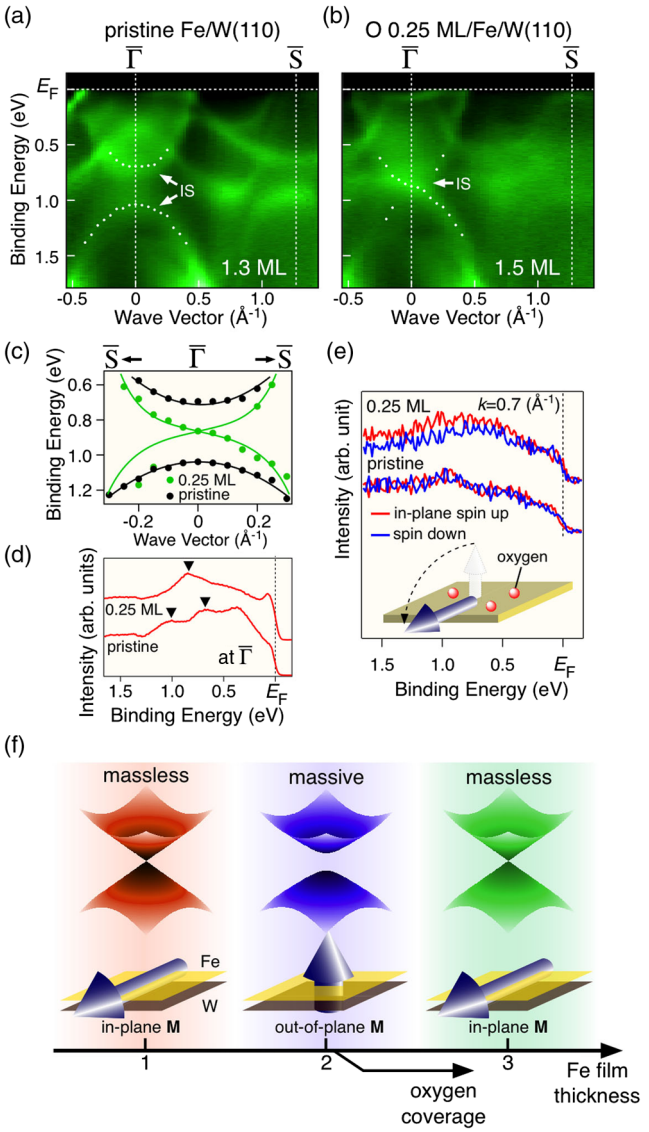

FIG. 3 (color online). (a),(b) Comparison of the ARPES intensity along the $\bar{\Gamma}$-$\bar{S}$ cut of Fe/W(110) for $d \sim 1.5$ ML upon oxygen adsorption of 0.25 ML. Oxygen coverage has been determined by the low-energy electron-diffraction (LEED) pattern showing the clear 2×2 spots. (c) Experimental band dispersion [same as dots in (a) and (b)] of the Dirac-cone band compared between pristine and oxygen-adsorbed samples. (d),(e) Comparison of EDC at the $\bar{\Gamma}$ point and spin-resolved EDC at $k = 0.7$ Å^{-1}, respectively, for pristine and oxygen-adsorbed Fe/W(110). Inset of (e) shows a schematic illustration of spin rotation upon oxygen adsorption onto Fe overlayers. The adsorption-driven spin reorientation would be triggered by the change in the strain of the Fe film and resultant change in the magnetic anisotropy [25]. (f) Schematic view of the Dirac-fermion mass switching and its link to the magnetization of Fe overlayers.

revealed by the Kerr magnetometry experiment [29]). Therefore, whatever the driving force of the change in the spin direction is, the massless or massive characteristics of Dirac fermions are directly related to the in-plane versus out-of-plane magnetization of Fe overlayers [Fig. 3(f)]. This demonstrates a strong coupling between the exchange field of iron and the Rashba SOC of tungsten at the interface.

The present result is a first direct experimental realization of the spin-dictated switching of Dirac-fermion mass in any known SOC systems including the TIs and the Rashba systems. Moreover, the observed Dirac gap of 340 meV is largest among these systems; it is more than twice as large as those so far achieved in the 3D TIs like Cr- and Mn-doped Bi_2Se_3 (~150 and ~50 meV, respectively) [19–21] in which the ferromagnetic moment is introduced by the doping of magnetic impurities into the crystal itself. In this regard, the magnetic proximity effect by attaching ferromagnetic layers onto the Dirac-fermion systems serves as an excellent approach for obtaining gigantic Dirac-fermion mass, and it would lead to a realization of novel quantum phenomena and stable operation of spintronic devices at higher temperatures. We therefore promote utilization of the magnetic proximity effect in various 3D TIs and Rashba systems. It is noted here that the larger Dirac gap in Fe/W(110) may be explained by the difference in the effective exchange field that the Dirac-like electrons feel and/or the difference in Curie temperature. In TIs, it is difficult to dope a large amount of magnetic impurities into the crystal without deteriorating the crystal quality and thereby topological characteristics, whereas this is not the case for the magnetic proximity effect. Moreover, Curie temperatures of magnetically doped TIs are usually well below room temperature (see, e.g., Refs. [19,20]), while that for 2-ML Fe (400–500 K) is much higher than that [30].

Strong coupling between the exchange field and the Rashba SOC, as revealed in this study, would promote the band engineering of the SOC systems. While the manipulation of exchange coupling by the Rashba SOC has been intensively examined thus far [31–35], the present finding provides a new pathway for the manipulation of the SOC system by the exchange field—an inverse approach to band engineering. This concept would be realized in a magnetic sensing in which the spin direction is determined only by proving the nonmagnetic interface without directly proving the magnetic layer itself. The electrical and optical probes may be useful for this purpose since they are sensitive to the charge excitations across the Dirac gap when the chemical potential is controlled to locate within the Dirac gap.

In conclusion, we reported spin-resolved ARPES study of Fe/W(110), and revealed an unexpectedly large energy gap of 340 meV at the Dirac-cone-like interface state. Moreover, we were able to switch the Dirac-fermion mass by controlling the direction of Fe spins, either by tuning the thickness of the Fe overlayer or by adsorbing oxygen on it. The present result suggests that the magnetic proximity effect is highly useful for realizing new spintronic devices in the hybrids of ferromagnetic and SOC systems.

We thank A. Takayama for her help in the ARPES experiments. This work was supported by JSPS (KAKENHI 23224010, 26287071, 25287079) and MEXT of Japan (Innovative Area "Topological Materials Science").

[1] X.-L. Qi and S.-C. Zhang, Rev. Mod. Phys. **83**, 1057 (2011).
[2] M. Z. Hasan and C. L. Kane, Rev. Mod. Phys. **82**, 3045 (2010).
[3] Y. Ando, J. Phys. Soc. Jpn. **82**, 102001 (2013).
[4] D. Pesin and A. H. MacDonald, Nat. Mater. **11**, 409 (2012).
[5] X.-L. Qi, R. Li, J. Zang, and S.-C. Zhang, Science **323**, 1184 (2009).
[6] R. Yu, W. Zhang, H.-J. Zhang, S.-C. Zhang, X. Dai, and Z. Fang, Science **329**, 61 (2010).
[7] E. McCann, Phys. Rev. B **74**, 161403(R) (2006).
[8] E. V. Castro, K. S. Novoselov, S. V. Morozov, N. M. R. Peres, J. M. B. Lopes dos Santos, J. Nilsson, F. Guinea, A. K. Geim, and A. H. Castro Neto, Phys. Rev. Lett. **99**, 216802 (2007).
[9] J. B. Oostinga, H. B. Heersche, X. Liu, A. F. Morpurgo, and L. M. K. Vandersypen, Nat. Mater. **7**, 151 (2008).
[10] K. Miyamoto, A. Kimura, K. Kuroda, T. Okuda, K. Shimada, H. Namatame, M. Taniguchi, and M. Donath, Phys. Rev. Lett. **108**, 066808 (2012).
[11] K. Miyamoto, A. Kimura, T. Okuda, K. Shimada, H. Iwasawa, H. Hayashi, H. Namatame, M. Taniguchi, and M. Donath, Phys. Rev. B **86**, 161411(R) (2012).
[12] J. Braun K. Miyamoto, A. Kimura, T. Okuda, M. Donath, H. Ebert, and J. Minár, New J. Phys. **16**, 015005 (2014).
[13] H. Mirhosseini, M. Flieger, and J. Henk, New J. Phys. **15**, 033019 (2013).
[14] H. Mirhosseini, F. Giebels, H. Gollisch, J. Henk, and R. Feder, New J. Phys. **15**, 095017 (2013).
[15] H. Bethge, D. Heuer, Ch. Jensen, K. Reshöft, and U. Köhler, Surf. Sci. **331–333**, 878 (1995).
[16] H. J. Elmers, J. Hauschild, H. Höche, U. Gradmann, H. Bethge, D. Heuer, and U. Köhler, Phys. Rev. Lett. **73**, 898 (1994).
[17] U. Gradmann, Surf. Sci. **116**, 539 (1982).
[18] See Supplemental Material at http://link.aps.org/supplemental/10.1103/PhysRevLett.115.266401 for the sample growth and the spin polarization of Dirac-cone band.
[19] C.-Z. Chang *et al.*, Phys. Rev. Lett. **112**, 056801 (2014).
[20] S.-Y. Xu *et al.*, Nat. Phys. **8**, 616 (2012).
[21] Y. L. Chen *et al.*, Science **329**, 659 (2010).
[22] A. Kubetzka, O. Pietzsch, M. Bode, and R. Wiesendanger, Phys. Rev. B **63**, 140407(R) (2001).
[23] M. Bode, O. Pietzsch, A. Kubetzka, S. Heinze, and R. Wiesendanger, Phys. Rev. Lett. **86**, 2142 (2001).
[24] N. Weber, K. Wagner, H. J. Elmers, J. Hauschild, and U. Gradmann, Phys. Rev. B **55**, 14121 (1997).
[25] T. Dürkop, H. J. Elmers, and U. J. Gradmann, J. Magn. Magn. Mater. **172**, L1 (1997).
[26] H. J. Elmers, J. Hauschild, and U. Gradmann, Phys. Rev. B **54**, 15224 (1996).
[27] T. Slezak *et al.*, Phys. Rev. Lett. **105**, 027206 (2010).
[28] F. S. Nogueira and I. Eremin, Phys. Rev. B **88**, 085126 (2013).
[29] H. J. Elmers, J. Hauschild, and U. Gradmann, Phys. Rev. B **59**, 3688 (1999).
[30] H. J. Elmers, J. Hauschild, H. Fritzsche, G. Liu, U. Gradmann, and U. Köhler, Phys. Rev. Lett. **75**, 2031 (1995).
[31] G. Yu *et al.*, Nat. Nanotechnol. **9**, 548 (2014).
[32] S. E. Barnes, J. Ieda, and S. Maekawa, Sci. Rep. **4**, 4105 (2014).
[33] I. M. Miron, K. Garello, G. Gaudin, P.-J. Zermatten, M. V. Costache, S. Auffret, S. Bandiera, B. Rodmacq, A. Schuhl and P. Gambardella, Nature (London) **476**, 189 (2011).
[34] T. Suzuki, S. Fukami, N. Ishiwata, M. Yamanouchi, S. Ikeda, N. Kasai, and H. Ohno, Appl. Phys. Lett. **98**, 142505 (2011).
[35] I. M. Miron *et al.*, Nat. Mater. **9**, 230 (2010).